CHROMATE INCORPORATION INTO CALCIUM CARBONATE MINERALS AND ASSOCIATED CHROMIUM ISOTOPE FRACTIONATION

A Thesis
Presented to
The Academic Faculty

By

Ashley Brady

In Partial Fulfillment
Of the Requirements for the Degree
Master of Science in Earth and Atmospheric Sciences

Georgia Institute of Technology

December 2017

CHROMATE INCORPORATION INTO CALCIUM CARBONATE MINERALS AND ASSOCIATED CHROMIUM ISOTOPE FRACTIONATION

Approved by:

Dr. Yuanzhi Tang
School of Earth and Atmospheric Sciences
Georgia Institute of Technology

Dr. Christopher Reinhard
School of Earth and Atmospheric Sciences
Georgia Institute of Technology

Dr. James Wray
School of Earth and Atmospheric Sciences
Georgia Institute of Technology

Date Approved: December 6, 2017

ACKNOWLEDGEMENTS

This project is supported by NASA Astrobiology Institute under Cooperative Agreement No. NNA15BB03A and NASA Exobiology grant NNX16AL06G. I appreciate the support from beamline scientist Dr. Ryan Davis at SSRL Beamline 4-1 on experimental setup. Portions of this research were conducted at the Stanford Synchrotron Radiation Lightsource (SSRL), SLAC National Accelerator Laboratory. Use of SSRL is supported by the U.S. Department of Energy, Office of Science, Office of Basic Energy Sciences under Contract No. DE-AC02-76SF00515. I would also like to thank my advisors, Dr. Yuanzhi Tang and Dr. Christopher Reinhard for their support and guidance throughout my Master's. Additionally, I would like to thank my family and friends for their support.

TABLE OF CONTENTS

LIST OF FIGURES

SUMMARY

The chromium (Cr) isotope system has recently gained interest as a paleoproxy for tracking atmospheric oxygen levels due to the presence of large isotope fractionations in association with redox reactions. One important assumption in the current framework is that redox reactions cause the most significant Cr isotope fractionations, and that these variations are faithfully preserved during the formation and burial of Cr-containing sedimentary rocks. Carbonate sediments are commonly used for Cr isotope paleoproxy studies due to their stratigraphic ubiquity and the potential that they record isotopic signals from shallow seawater. It is critical to investigate and understand potential isotope fractionations caused by Cr incorporation into carbonate minerals for paleoproxy improvement. We investigated Cr isotope fractionation during Cr(VI) co-precipitation with different calcium carbonate mineral phases (aragonite, calcite, and amorphous calcium carbonate), with a specific focus on the effects of precipitation rate and aqueous Cr concentration. Scanning electron microscopy (SEM) and X-ray diffraction (XRD) were used to determine the mineral phase and morphology of the solid phase precipitates. X-ray adsorption spectroscopy (XAS) was used to determine oxidation state and the local bonding environments of incorporated Cr ions. Chromium isotope fractionation was measured using a multi-collector inductively coupled plasma mass spectrometer (MC-ICP-MS). The isotope fractionation signatures measured from this preliminary study are significant when compared to previous Cr isotope fractionation measured in carbonate sediments and should be considered in further attempts to better constrain isotopic mass balance of Cr in modern and ancient oceans.

CHAPTER 1

INTRODUCTION

Atmospheric oxygen evolution is key to understanding the evolution of Earth's habitability as a planet. The original composition of the Earth's atmosphere was composed of hydrogen, sulfide, methane, and carbon dioxide and slowly evolved to include oxygen (Trail et al., 2011). The main contributing process that increased oxygen in the atmosphere was photosynthetic production of oxygen via microbial productivity (Kasting et al., 1985; Raymond and Segre, 2006). The Great Oxidation Event (GOE) is the atmospheric oxygen concentration increase as defined by the loss of sulfur mass independent fractionation (Bekker et al., 2004; Canfield, 2005; Holland, 2002, 2006). Although the change in atmospheric oxygen concentration can be seen through sulfur isotope records and other geologic evidence, precise changes in atmospheric oxygen concentration cannot be constrained by sulfur isotope fractionation alone (Kump, 2008). Other proxies, such as molybdenum (Mo) and chromium (Cr), have opportunity to serve as alternative proxies for determining atmospheric evolution and its evolving oxygen concentration (Arnold et al., 2004; Frei et al., 2009; Reinhard et al., 2013). These proxies have the possibility of origin in a larger variety of rocks and detecting smaller atmospheric oxygen concentration changes as opposed to traditional sulfur mass isotope fractionation (Frei et al., 2009; Gilleaudeau et al., 2016). The goal of this study is to further examine an assumption made for the Cr isotope system paleoproxy to determine atmospheric oxygen concentration and possibly provide corrections for errors within the assumption.

1.1 Previous Proxies

Geologic evidence was first used to determine change in atmospheric oxygen concentration. One feature that shows little available oxygen is a lack of oxidized Fe^{2+} in paleosols before 2.5 billion years ago (Ga) (Ohmoto, 1996). Some geologic features that show atmospheric oxygen during and after the GOE include the absence of red oxidized beds, the presence of banded iron formations (BIFs), and the presence of detrital uraninite and pyrite in sediments (Konhauser et al., 2011; Mukhopadhyay et al., 2014; Sheldon, 2006). The presence of these different geologic features gave insight into an earlier Earth and possible atmospheres during their formation.

Sulfur mass independent fractionation (MIF) has been used to determine the minimum atmospheric oxygen concentration of the Archean (Pavlov and Kasting, 2002). Conditions that have been shown to create MIF in sulfur samples include low atmospheric oxygen, high sulfur gas concentrations in the atmosphere, and large concentrations of reducing gases (Kump, 2008). The decrease in sulfur fractionation (Farquhar and Wing, 2003) is observed because sulfate concentrations were increased after the GOE when atmospheric oxygen concentration increased (Lyons and Gill, 2010; Pavlov and Kasting, 2002). A change in fractionation, from -2 to +8 ‰ before GOE and -0.5 to +1 ‰ after GOE, was measured and observed in pyrite and barite samples and correlated to atmospheric oxygen concentration (Holland, 2006). However, the precision of sulfur isotopic fractionation is not accurate to determine the concentration of atmospheric oxygen, other than to distinguish the presence of oxygen greater than 10^{-5} present atmospheric levels (PAL; (Bekker et al., 2004).

Carbon isotopic fractionation has also shown large positive signals between 2.22 and 2.06 billion years ago (Karhu and Holland, 1996). Prior to 2.2 Ga signals were approximately 0‰ in carbonates and increased dramatically to +30‰ around 2.2 Ga (Bekker et al., 2008; Karhu and Holland, 1996). These high carbon fractionation values are also found in work by Schidlowski and others (1976) with dolomite carbon fractionation mean of 8.2‰. The positive increase in fractionation is due to organic matter degradation and burial surpassing oxidative weathering rates (Kump et al., 2011). Although this supports a dramatic change in atmospheric oxygen concentration, this proxy is not definitive in quantifying atmospheric oxygen concentration for the time during formation of these carbonate sediments (Bekker and Holland, 2012; Karhu and Holland, 1996).

Molybdenum (Mo) fractionation has also been proposed to determine oceanic oxygen concentrations (Arnold et al., 2004). Ocean redox conditions may be reflected by Mo measurements due to the mobility of Mo by oxidation. Under euxinic conditions, Mo is removed from solution and therefore precipitated out of solution. Mo fractionation from sorption onto Mn oxyhydroxide is -2.7‰ whereas Mo fractionation from sorption onto Fe oxyhydroxide is only -1.1‰ (Barling and Anbar, 2004). Mn oxyhydroxides need an oxidizer to be produced, and it is suggested 0.1 PAL is required for Mn oxyhydroxide production (Planavsky et al., 2014b). Mn oxides can also be produced via microbial reactions and result in faster kinetics to produce these manganese oxides (Tebo et al., 2005). Isotopic fractionation of Mo investigation has shown Mo to be redox sensitive, and therefore could give better insight into the atmospheric oxygen concentration (Arnold et al., 2004; Duan et al., 2010; Wille et al., 2007). Mo fractionation shows similar sensitivity to chromium (Cr) fractionation, and one day both Cr and Mo could be used in conjunction

with one another to constrain atmospheric oxygen evolution. Cr fractionation has the potential to serve as a powerful paleoproxy for ancient atmospheric O_2.

1.2 Cr Isotope System as Paleoproxy

The chromium (Cr) isotope system has recently emerged as a promising paleoproxy for atmospheric oxygenation since its introduction in 2009 by Frei et al (2009). Several further studies have investigated Cr isotope fractionation in shales and carbonate samples from 3.2 to 0.7 billion years (Ga) in regards to redox processes and their possible connections to atmospheric oxygenation (Crowe et al., 2013; Frei et al., 2009; Planavsky et al., 2014a; Planavsky et al., 2014b; Reinhard et al., 2013). Chromium isotopic fractionation was first studied in regards to environmental contamination (Bartlett and James, 1979). Cr commonly occurs in nature as Cr(III) or Cr(VI) (Fendorf, 1995). Cr(VI) is toxic and soluble whereas Cr(III) is a micronutrient and typically insoluble, excluding rare environments such as ligand-complexed Cr(III) and soluble Cr(III) (Katz and Salem, 1994; Kotas and Stasicka, 2000). The four masses of chromium and their environmental percentages include 50 (4.35%), 52 (83.8%), 53 (9.50%), and 54 (2.37%), but ^{52}Cr and ^{53}Cr are most commonly used in isotope fractionation studies (Adriano, 1986; Barnhart, 1997). During redox processes, it was found that fractionation would occur during the reduction or oxidation of chromium in the environment (Crowe et al., 2013; Dossing et al., 2001; Frei et al., 2009). Unlike iron which fractionates due to sorption and incorporation processes (Johnson et al., 2008), Cr fractionation appears to be redox-dependent. Two different modes of isotopic fractionation exist, kinetic and equilibrium. Kinetic fractionation occurs when the system is not allowed to isotopically equilibrate and

therefore masses will differentiate dependent upon the reaction (i.e. light isotopes concentrated in reaction products due to faster kinetics of weaker bonds; (Schauble, 2004). Equilibrium fractionation occurs when the system is at isotopic equilibrium and allowed to exchange to achieve the highest stability bonds (Schauble, 2004). The average amount of fractionation for reduction reactions are between -3 to -4.5‰ and +1 to +5‰ (Dossing et al., 2001; Ellis et al., 2002), while the average amount of fractionation for oxidation reactions are -0.9 to +4.9‰ (Crowe et al., 2013; Frei et al., 2009; Reinhard et al., 2014). The positive fractionation observed in nature is evidence of heavier Cr preference to lighter Cr during redox processes. Traditionally, more research was focused on the reduction of Cr(VI) to Cr(III) as this has environmental relevance with regards to Cr contamination (Ellis et al., 2002; Milacic and Stupar, 2006). Using isotopic fractionation of chromium in areas of contamination can determine the degree of reduced contamination (Bartlett, 1991; Milacic and Stupar, 2006). Chromium fractionation can be used as a long-term proxy to understand redox reactions that have occurred, and this concept can be used to look at redox processes with Cr and atmospheric oxygen concentration.

The framework of this isotope system is based on previous observations that Cr isotopic fractionation is most significant during biogeochemical processes involving changes in its two dominant oxidation states, Cr(III) and Cr(VI) (Crowe et al., 2013; Dossing et al., 2001; Frei et al., 2009; Milacic and Stupar, 2006; Planavsky et al., 2014b; Reinhard et al., 2013; Zink et al., 2010). Cr(III) is commonly found in the environment as low solubility and low mobility solid phases, whereas Cr(VI) species are typically soluble thus highly mobile (Bagchi et al., 2002; Bartlett, 1991). The mechanisms by which this paleoproxy relies upon is illustrated in Figure 1. In brief, Cr(III) from mafic rocks is weathered and oxidized to

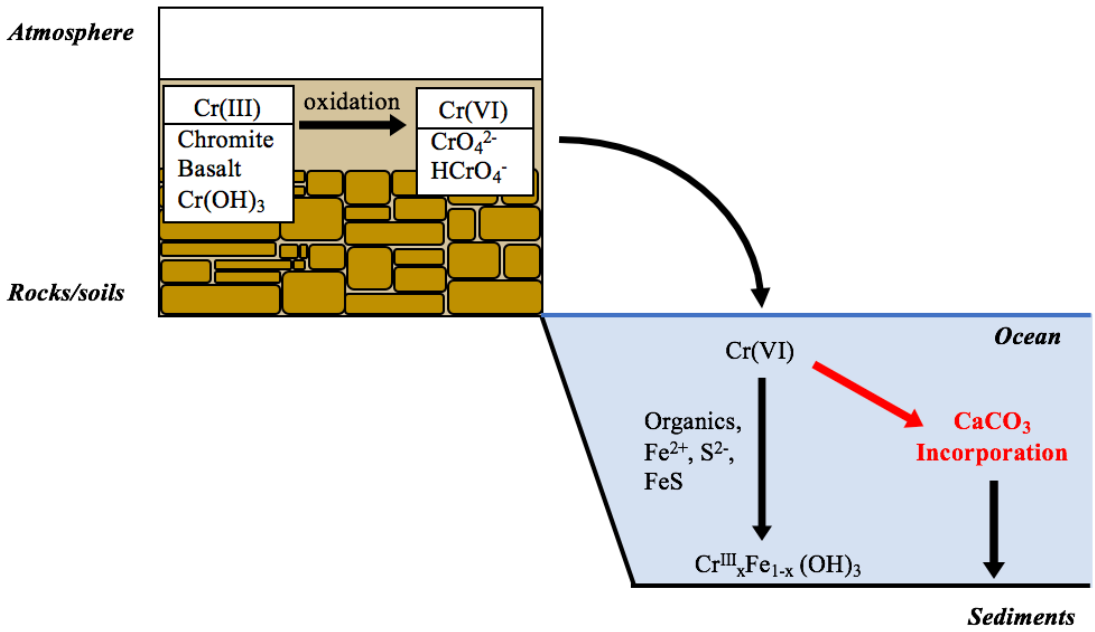

Figure 1: Schematic illustration of the Cr cycle as related to the Cr isotope system as a paleoproxy for oxygenation, modified from Frei et al (2009). Red highlights show the mineral incorporation pathway (i.e. incorporation of soluble Cr(VI) into calcium carbonate minerals) examined in this study.

Cr(VI) by manganese (Mn) oxides, the most significant environmental oxidants of Cr(III) (Bartlett and James, 1979; Eary and Rai, 1987; Fendorf, 1995). Following this oxidative mobilization process, which was previously shown to generate large Cr isotope fractionation (Bain and Bullen, 2005), dissolved Cr(VI) is transported into marine environments, reduced to Cr(III), and precipitated and preserved in sediments as Cr(III)-Fe(III)-hydroxides (Buerge and Hug, 1997; Fendorf, 1995; Sass and Rai, 1987).

In regards to atmospheric oxygen concentration proxies, Cr isotope fractionation is dependent upon the fractionation of Cr when undergoing the oxidation of Cr(III) to Cr(VI) by manganese oxides (MnOx) (Frei et al., 2009). Measuring Cr fractionation signal in rocks formed during the GOE may be indicative of atmospheric oxygen concentration by tracing

the amount of oxidation that occurred to the Cr before being precipitated as Cr, Fe hydroxides (Crowe et al., 2013). The previous environmental contamination research laid the groundwork for paleoproxy applications by providing redox as a single source of fractionation that could be quantified and therefore resemble atmospheric oxygen concentration (Izbicki et al., 2012). For this proxy to effectively trace minute atmospheric oxygen concentration changes, there are some general assumptions that must be made in regards to the processes by which Cr undergoes and the oxidation of Cr within the crust (Frei et al., 2009). Figure 1 demonstrates these assumptions first outlined by Frei and others (2009). The first assumption is that the only oxidizer that has rapid kinetics to oxidize Cr(III) to Cr(VI) are MnOx. The second assumption is that the only source of Cr isotopic fractionation to be measured in the rock record is directly correlated to the redox processes that the rock has undergone after weathering through deposition in the ocean. The goal of my Master's research is to determine if the second assumptions is valid, and if not how we can adjust the proxy to demonstrate my findings and more accurately project the atmospheric oxygen concentration.

The first assumption shown in Figure 1 is that the only oxidizer of Cr(III) to Cr(VI) is the presence of MnOx. The formation of these manganese oxides is solely dependent upon the atmospheric oxygen concentration above 0.1 PAL, as manganese exposure to atmospheric oxygen will be oxidized to MnOx (Tebo et al., 2004). This MnOx is then able to oxidize Cr(III) to Cr(VI), thus providing a direct correlation of atmospheric oxygen concentration to the isotopic fractionation signature observed in chromium-bearing Cr, Fe hydroxides (Ellis et al., 2002; Izbicki et al., 2012). Oxygen was thought to be the most favorable oxidizer of Cr(III) to Cr(VI), but it has been shown in previous studies that the

kinetics for this reaction are much slower than manganese oxides and essentially show that all oxidation of Cr(III) is done in the presence of MnOx (Apte et al., 2006). It has also been shown in previous studies that there is a possibility that Cr(III) can be oxidized by other reactive oxygen species, such as hydrogen peroxide (Baloga and Earley, 1961; Eary and Rai, 1987; Lindsay et al., 2012; Pettine and Millero, 1990). The oxygen necessary in the atmosphere to produce MnOx also provides a limitation on the lower bound of the concentration of atmospheric oxygen that the Cr isotope system proxy can detect and quantify. The lower constraint for atmospheric oxygen needed to oxidize Mn is controversial with values ranging from 10^{-5} PAL based on thermodynamic limitations (Frei et al., 2016) to 0.1 to 1% PAL based on kinetic limitations and soil residence times (Planavsky et al., 2014b) and 0.03 to 0.1% PAL based on Cr export without Fe(II) reduction (Crowe et al., 2013).

The second assumption highlighted in Figure 1 is the simple process by which weathered Cr(III) is transported to and deposited in the ocean. After the oxidation of Cr, discussed prior, the soluble Cr(VI) is assumed to undergo quantitative reduction by Fe(III) in the water column and that the insoluble Cr(III) is then deposited into sediments as Cr, Fe hydroxides (Fendorf, 1995; Sikora et al., 2008). It is assumed that during the reduction of Cr(VI) to Cr(III) that there is no fractionation, inferring that all the Cr(VI) is reduced to Cr(III) therefore no signal would be observed for this reduction reaction (Dossing et al., 2001). There are a few processes that could possibly occur to contradict this assumption. First, Cr(VI) may be directly incorporated into different calcium carbonate precipitates formed from biotic or abiotic sources (Gilleaudeau et al., 2016; Rodler et al., 2015; Tang et al., 2007; Wang et al., 2016). It has been shown that other anions, such as selenate,

sulfate, and boron oxyanions which are similar size to chromate, will incorporate at the carbonate site and may cause stress on the surrounding crystalline lattice (Kitano et al., 1978; Reeder et al., 1994; Staudt et al., 1994). There are two different orientations that selenate can incorporate into the structure including axial and non-axial positions (Reeder et al., 1994). If this Cr(VI) incorporation can create a fractionation signal, then it could be implied as an indicator of atmospheric oxygen presence. It is also important to consider the different calcium carbonate phases that Cr(VI) could incorporate itself into the structure. Aragonite, calcite, and amorphous calcium carbonate (ACC) are commonly found in marine environments and can form from abiotic or biotic sources (Wang et al., 2016). If Cr incorporates itself differently as specified by the mineral source as well as fractionation signature is different in different mineral sources, then this is important to consider and quantify when examining carbonate sediments for Cr isotopic measurements. Second, it is assumed that all Cr(VI) is reduced to Cr(III), and if this is not the case then there would be a fractionation signal from this reduction process that may not be considered when determining atmospheric oxygen concentration utilizing this proxy (Frei et al., 2009). Third, the process of diagenesis is not considered as a possible source of fractionation, but it has been shown in previous stable isotopic fractionation measurements, such as Fe isotopic fractionation, that fractionation can be induced by the formation of rocks from sediments (Banner and Hanson, 1990; Goldhaber and Kaplan, 1980; Johnson et al., 2008). The temperatures and pressures that sediments must undergo to create sedimentary rocks can facilitate strain in the sediments and cause another signal of Cr isotopic fractionation. Although these are all assumptions that should be considered before utilizing this proxy,

this study will investigate the incorporation of Cr(VI) into carbonate mineral phases that could produce fractionation and better constrain the isotopic effects.

1.3 Previous Cr Isotope Paleoproxy Results

In general, results from the Cr isotope system align with other paleoproxy constraints for atmospheric oxygen evolution during the GOE in geologic samples including banded iron formations (BIFs), shales, and anoxic sediments (Crowe et al., 2013; Frei et al., 2009; Planavsky et al., 2014a; Planavsky et al., 2014b). Previous atmospheric oxygen constraints from sulfur (S), carbon (C), and molybdenum (Mo) isotope systems paleoproxies agree with that of Cr isotope findings (Anbar et al., 2007; Karhu and Holland, 1996; Planavsky et al., 2014b). The consensus among S, C, Mo, and Cr isotope systems show that prior to 2.5 Ga, atmospheric oxygen concentration was below 10^{-5} PAL and increased around the GOE to 10^{-5} PAL (Bekker et al., 2004; Kump, 2008; Lyons et al., 2014). The Cr isotope system allows for atmospheric oxidation predictions that may be finer scale than previous paleoproxies, and Cr can be found in carbonate sediments as well as BIFs and shales (Frei et al., 2009). More recently, Cr isotope fractionation has been measured in modern carbonate sediments to determine the accuracy of the Cr isotope signature in comparison with modern marine environments (Reinhard et al., 2014; Wang et al., 2016), and biogenic carbonates have been found to vary from seawater Cr isotope signature (Mohanta et al., 2016; Pereira et al., 2016). These results indicate that clays in euxinic marine environments and calcitic foraminifera in marine environments can provide seawater δ^{53}Cr composition measured previously to be -0.4 to +1.5 ‰ (Bonnand et al., 2013; Pereira et al., 2016; Reinhard et al., 2014; Scheiderich et al., 2015; Wang et al.,

2016). However, much still remains unknown on the potential impacts of redox-independent processes, such as mineral incorporation, on Cr isotope fraction.

Indeed, carbonate minerals, such as calcite and aragonite, are ubiquitous and commonly used in paleoproxy studies (McKay and Pedersen, 2014; Reinhard et al., 2014; Scott and Lyons, 2012). They form abundantly in marine environments and can provide geologic record of atmospheric oxygen where shales and BIFs are limited, such as the mid-Proterozoic (Gilleaudeau et al., 2016). Numerous types of cations (e.g. uranyl, Mn^{2+}, Sr^{2+}, Cd^{2+}, Cu^{2+}, Zn^{2+}, and Co^{2+}) can incorporate into calcite and aragonite and the mechanisms have been extensively studied (Elderfield et al., 1996; Elzinga and Reeder, 2002; Lorens, 1981; Menadakis et al., 2009; Mucci and Morse, 1983; Reeder et al., 2000). Anions (e.g. sulfate, borate, arsenate, and selenate) can also incorporate into calcite (Bardelli et al., 2011; Hemming et al., 1998; Kontrec et al., 2004; Lamble et al., 1995; Renard et al., 2013; Staudt and Schoonen, 1995), and chromate, arsenate, and selenate were shown to substitute at the carbonate site (Bardelli et al., 2011; Lamble et al., 1995; Rodler et al., 2015; Staudt et al., 1994; Tang et al., 2007). In a recent study, isotopic fractionation of Cr was measured during chromate incorporation into abiotic calcite (DePaolo, 2011; Rodler et al., 2015). Although this study provided exciting evidence of Cr isotope fractionation via calcite mineral incorporation Rodler et al. (2015), the presence of interfering solid phases other than calcite (e.g. halite, vaterite, silica gel) hindered the interpretation of the isotope results. Previous studies have also shown that biogenic calcites have enriched ^{53}Cr within their structure (Dixon et al., 2013) in agreeance with previous studies of synthesized calcite. Although many studies have studied anion incorporation into calcite, the lack of anion incorporation into other calcium carbonate mineral phases exists and will be addressed in

this study. It is also important to constrain the amount of chromium incorporated into these different calcium carbonate mineral phases. If incorporation can produce fractionation, then it is vital to understand this process (incorporation and fractionation) with regards to the Cr isotope system as a paleoproxy. Constraining the fractionation associated with carbonate incorporation allows for better understanding of the global Cr cycle and further applications of the Cr isotope system as a paleoproxy.

This study aims to systematically examine the incorporation of chromate into various calcium carbonate mineral phases and the associated isotopic fractionation. Chromate is the mobile Cr(VI) speciation upon weathering of Cr(III)-containing minerals. Three representative calcium carbonate phases of interest are aragonite, calcite, and amorphous calcium carbonate (ACC). These phases have varying structural flexibility and/or crystallinity. Carbonate sediments are found along continental shelves, and high-magnesian calcite and aragonite are the dominant carbonate minerals in these deposits (Friedman, 1964; Lee and Buller, 1972). Abiotic carbonate grains are limited to warm-water shelves. For biogenic carbonate minerals, foraminifera and molluscs are ubiquitous while other species (e.g. barnacles, ostracods, sponges, and corals) are limited (Lee and Buller, 1972). Previous studies have demonstrated that ACC can transform to aragonite in the presence of Mg^{2+} (Zhang et al., 2012) or calcite at 7.5 to 25 °C (Rodriguez-Blanco et al., 2011). Studies have also revealed the role of biogenic ACC as a precursor for calcite (Beniash et al., 1997; Politi et al., 2004; Politi et al., 2008) or aragonite exoskeletons (Weiss et al., 2002). Ca^{2+} ions are nine coordinated in aragonite and six coordinated in calcite (Reeder, 1983). ACC has a much more flexible structure dominated by porous openings (Goodwin et al., 2010). These differences in crystal lattice may affect Cr(VI) incorporation

and subsequent Cr isotopic fractionation and should be systematically investigated in order to better calibrate the Cr isotope system for its applications in carbonate sediment records.

CHAPTER 2

EXPIRMENTAL METHODS

2.1 Coprecipitation Experiments

All glasswares was acid washed with 10% HCl acid and rinsed with deionized (DI) water (18.2 MΩ). All chemicals were of ACS grade or higher. All experiments were conducted under room temperature (22 ºC).

Synthesis of Cr(VI)-doped calcite and aragonite samples followed the constant addition method described by Reeder et al. (2000) and Tang et al. (2007). For calcite synthesis, solution A containing 0.1M $CaCl_2 \cdot 2H_2O$ and solution B containing 0.1M Na_2CO_3 were added separately by syringe pump at varied pump rates (5–400µL/min). These solutions were added to a beaker containing varied concentrations of K_2CrO_4 (0.01–5mM), 0.1M NaCl, 0.007M $NaHCO_3$, and 0.007M $CaCl_2$. Water saturated air was continuously bubbled through the suspension. To synthesize aragonite, 0.007M $MgCl_2$ was added to the beaker described above. For all experiments, pH of the reaction suspension was periodically monitored, and the experiment concluded when the pH stabilized around 8.3. Typical reaction times ranged from 2 to 20 hours. Cr(VI) concentration of the filtrate was measured using DPC method (Eaton et al., 1995) at 540 nm using a UV-visible spectrophotometer (Cary60, Agilent). At the end of an experiment, the reaction suspension was vacuum filtered, rinsed with DI, and the solid precipitates dried in an oven at 50 ºC. A portion of the dried solids were dissolved in 10% nitric acid for Cr(VI) concentration analysis. Filtrate was diluted and analyzed for Cr(VI) concentration using DPC method. Dried solid was broken into smaller pieces using pestle and mortar for XRD and SEM

analysis. For Cr isotope analysis, filtrates were stored frozen and the solids stored in a desiccator until analysis.

Cr(VI)-doped ACC samples were synthesized following Koga et al. method (1998). Two bottles containing 0.1M Ca^{2+} solution ($CaCl_2 \cdot 2H_2O$) and 0.1M CO_3^{2-} solution (Na_2CO_3) were placed in a refrigerator overnight, after which 100 mL of each solution was quickly combined into a beaker under vigorous stirring. The reaction was allowed to last for 2 minutes and the resulting white precipitates were vacuum filtered (0.45 μm) and rinsed with DI and acetone. The filtrate was analyzed for Cr(VI) concentration using the DPC method. The resulting solids were air dried under high air flow for 15 minutes. A portion of the solids was digested in 10% nitric acid for Cr(VI) concentration analysis. For Cr isotope analysis, liquid samples were stored at -20 degrees C. The solids were acidified using HNO_3 either immediately after experiments (referred to as ACC fresh) or after 1 day in dried environment (referred to as ACC aged), and the digestates were stored at room temperature until Cr isotope analysis. Previous studies have shown that ACC transforms into calcite at 7.5 to 25 °C (Rodriguez-Blanco et al., 2011) and aragonite when exposed to high concentrations of Mg^{2+} (Zhang et al., 2012).

Solid samples were further characterized by X-ray diffraction (XRD), scanning electron microscopy (SEM), X-ray absorption spectroscopy (XAS), and Cr isotope analysis to determine the phase, morphology, local structure, and isotope composition, as detailed below. Cr partition coefficients were calculated using the following equation:

$$K_d = \frac{[Cr(VI)]_{solid}\ (ppm)}{[Cr(VI)]_{final\ solution}\ (ppm)}. \qquad \text{(Eq. 1)}$$

2.2 X-ray Absorption Spectroscopy (XAS) Analysis

Cr K-edge XAS data were collected for Cr-doped calcite, aragonite, and ACC at beamline 4-1 of the Standard Synchrotron Radiation Lightsource (SSRL; Menlo Park, CA). Sample powders were packed in acrylic sample holders and scans were collected at room temperature in fluorescence mode using a Ge multi-element detector. Energy calibration used Cr foil. Monochromators were detuned by 40% to avoid higher order harmonics. Multiple scans were collected for each sample, including both X-ray absorption near edge structure (XANES) region. Consecutive scans of the XANES region were compared and beam induced photo reduction was not observed throughout the experiments.

2.3 Cr Isotopic Analysis

Cr fractionation measurements were done with a Thermo Neptune Plus multi-collector ion coupled plasma mass spectrometer (MC-ICP-MS) at Yale Metal Geochemistry Center. The modifications made to the instrument include a Pfeifffer OnToolBoster 150 Jet Pump that enables the usage of a Jet sampler cone and an X skimmer cone to maximize ion transmission efficiency. To further boost the signal, an Apex IR introduction system was used. Faraday cups are connected to 10^{11} Ω amplifiers to measure masses 49, 50, 51, 52, 53, 54, and 56 simultaneously. The samples underwent column separation (Wang et al., 2016) and double spike prior to analysis by the MC-ICP-MS. Samples were also bracketed with spiked standards (NIST SRM 979) of similar Cr concentration and then underwent double spike calculation after corrections were made from the bracketed spiked standard. Extracted ratios are converted to δ^{53}Cr by normalizing to standard SRM 979 using the following equation:

$$\delta^{53}Cr = [(^{53}Cr/^{52}Cr)_{sample}/(^{53}Cr/^{52}Cr)_{SRM\ 979}) - 1)\times 1000 \qquad \text{(Eq. 2)}$$

$\Delta^{53}Cr$ values were determined by the following equation:

$$\Delta^{53}Cr = \delta^{53}Cr_{sample} - \delta^{53}Cr_{initial} \qquad \text{(Eq. 3)}$$

where $\delta^{53}Cr_{initial}$ was of K_2CrO_4 starting material, +0.01‰.

CHAPTER 3

RESULTS

3.1 Batch Precipitation Results

XRD analysis verified that the solid phases formed during calcite and aragonite precipitation experiments were indeed calcite and aragonite, except for Cr(VI)-calcite experiment conducted at high precipitation rate of 400μL/min, which show the presence of minor amounts of aragonite (Figures 2 and 3). These results are consistent with SEM observations (Figure 4). All aragonite experiments produced aragonite crystals with spiked morphology. For calcite experiments conducted at all concentrations (0.1 – 5mM) and low precipitation rate (≤250μL/min), precipitated mineral phases appear as the typical rhombohedral crystals of calcite. For calcite experiment conducted at 400μL/min precipitation rate, minor amounts of aragonite were also observed in addition to calcite, consistent with XRD results.

Cr incorporation into calcite, aragonite, and ACC were measured by determination of Cr(VI) in solid and determination of K_d by Equation 1 (Figures 5 and 6). Results are displayed at constant pump rate (150μL/min) at various Cr(VI) concentrations (0.005 – 5mM; Figure 5) and constant Cr(VI) concentration (1mM) at various pump rates (5 – 400μL/min; Figure 6). As $Cr(VI)_{final\ in\ solution}$ increases, in calcite and aragonite $Cr(VI)_{solid}$ also increases (Figure 5a). ACC however shows an increase in $Cr(VI)_{solid}$ from 0.1 – 5mM $Cr(VI)_{final\ in\ solution}$. The K_d does not have any correlation with $Cr(VI)_{final\ in\ solution}$ (Figure 4b), but does fall in a range between 0 - 70. For 1mM Cr(VI) and various precipitation rates, in general it appears that $Cr(VI)_{solid}$ increases as the precipitation rate increases for calcite

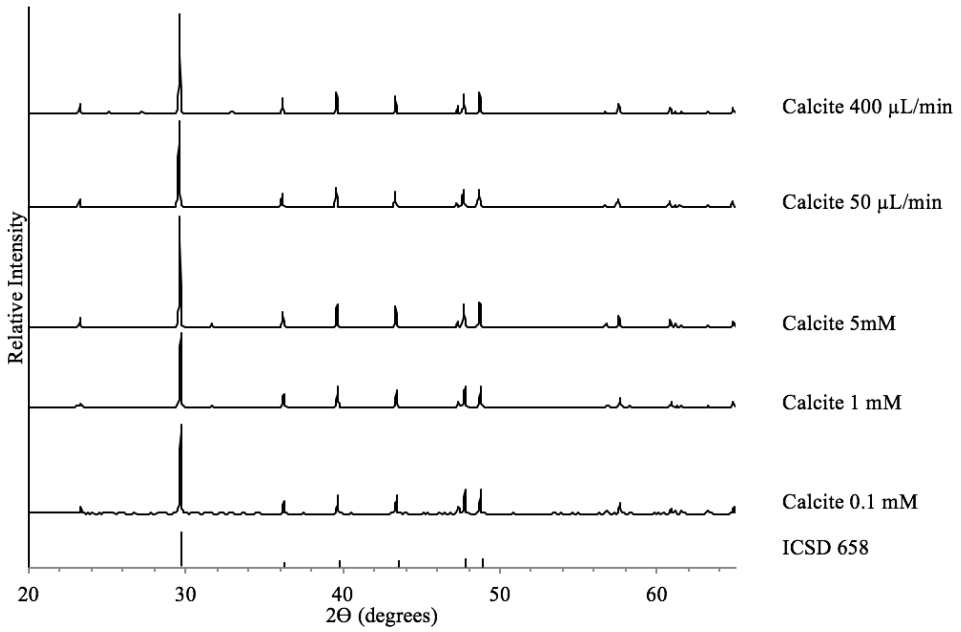

Figure 2: XRD patterns (Cu Kα radiation) of calcite samples synthesized in the presence of varied Cr(VI) concentrations (0.1, 1, 5 mM, pump rate 150µL/min) and syringe pump rates (50 and 400 µL/min, Cr(VI) concentration 1 mM).

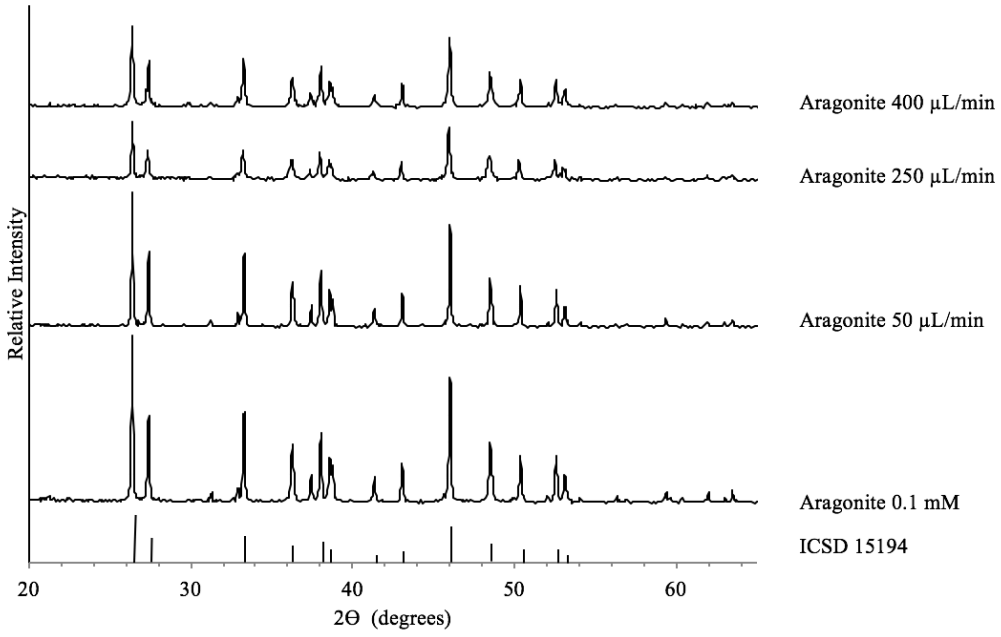

Figure 3: XRD patterns (Cu Kα radiation) of aragonite samples synthesized in the presence of varied Cr(VI) concentrations (0.1mM, pump rate 150µL/min) and syringe pump rates (50, 250, and 400 µL/min, Cr(VI) concentration 1 mM).

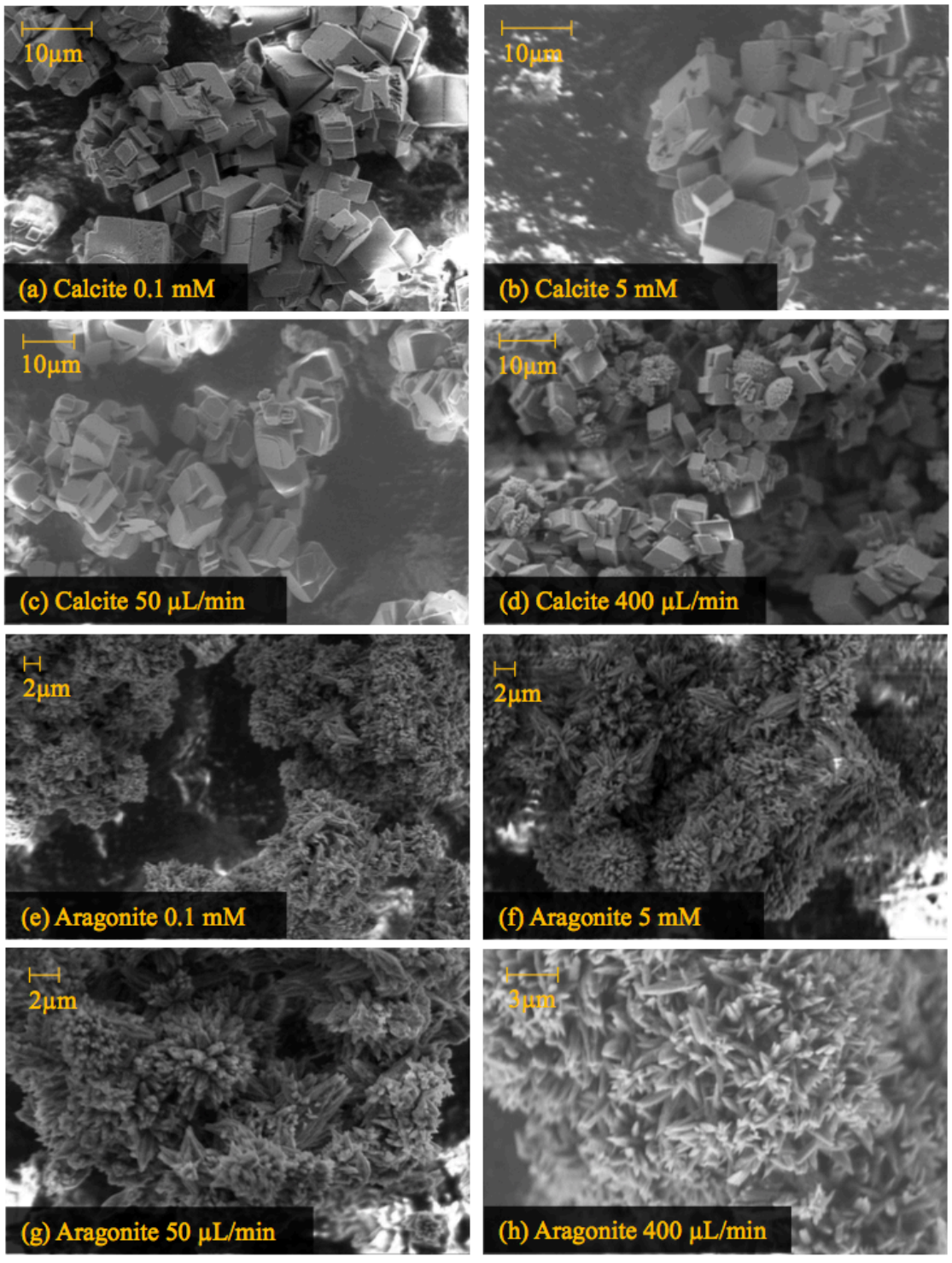

Figure 4: SEM images of Cr(VI)-doped calcite (a, b, c, and d) and aragonite (e, f, g, and h) samples synthesized at 0.1 or 5mM Cr(VI) concentration (150µL/min pump rate; a, b, e, and f) or at pump rates of 50 or 400 µL/min (1mM Cr(VI); c, d, g, and h).

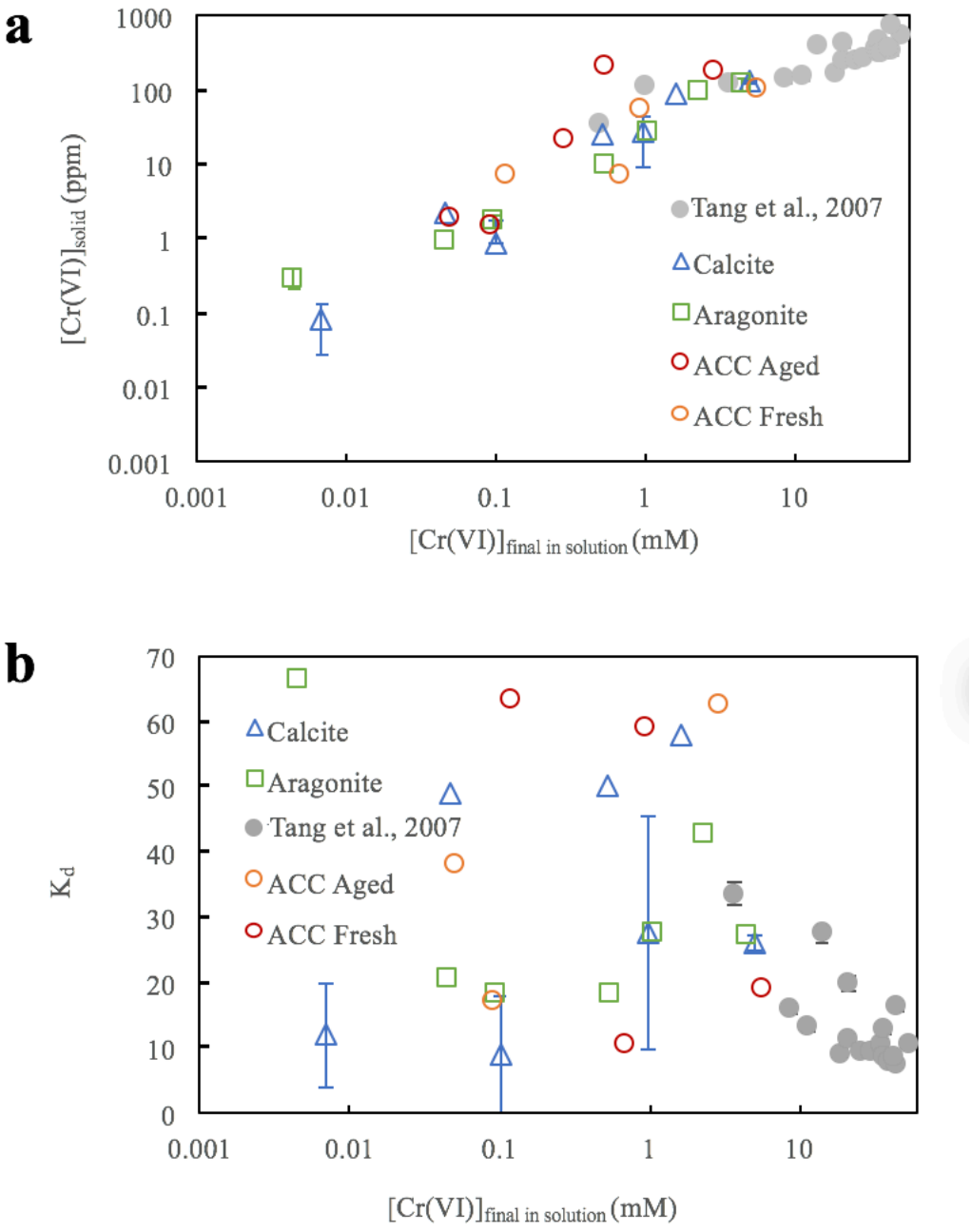

Figure 5: Cr(VI) concentration (a) and partition coefficient K_d (b) in calcite, aragonite, and ACC as a function of Cr(VI) concentration in the final solution when experiments reached near steady state. Pump rate = 150 µL/min. Error bars represent duplicate experiments.

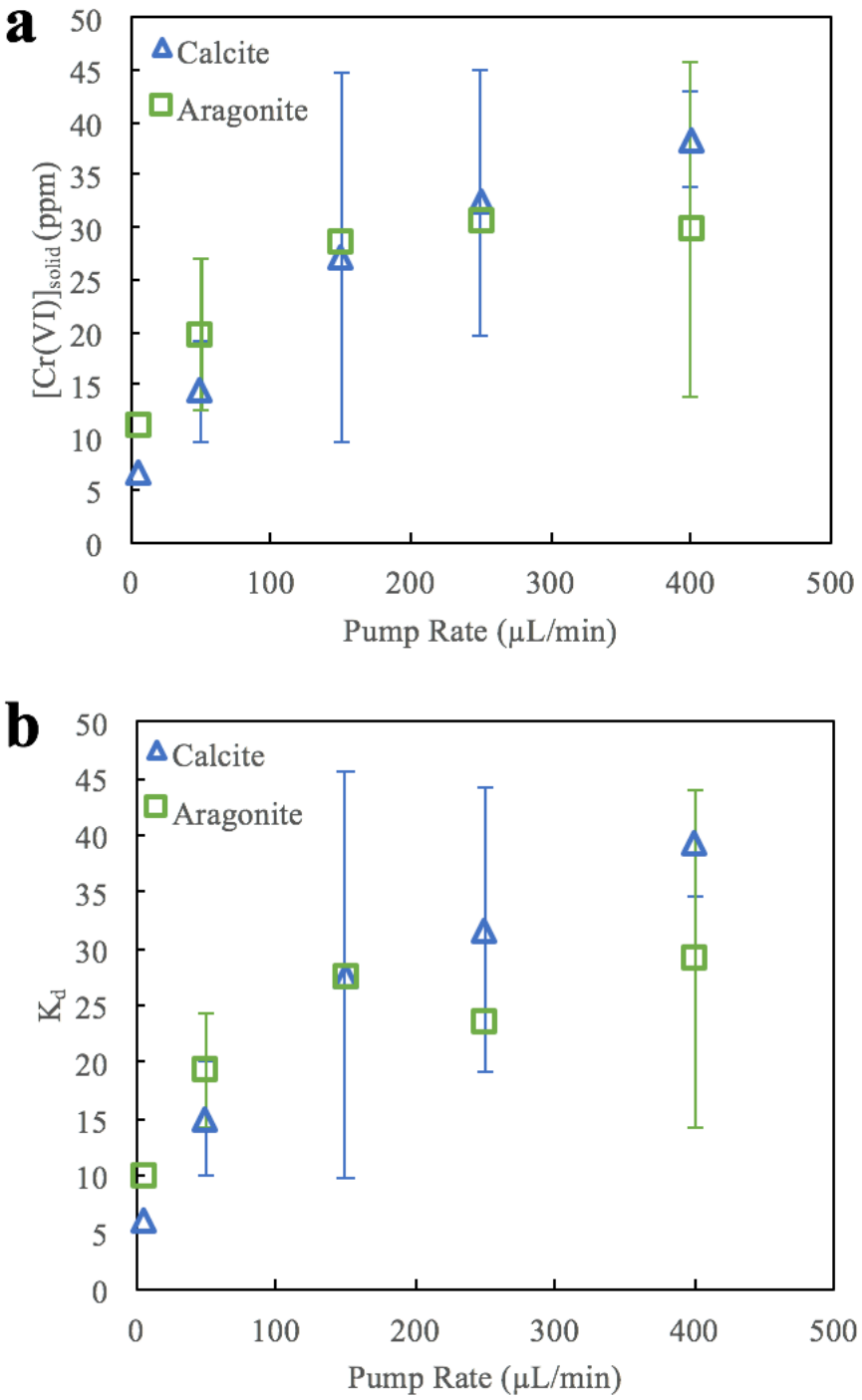

Figure 6: Cr(VI) concentration (a) and partition coefficient Kd (b) in calcite and aragonite as a function of pump rate when experiments reached near steady state. Cr(VI) = 1mM. Error bars represent duplicate experiments.

(Figure 6a). It also appears that aragonite $Cr(VI)_{solid}$ increases until 150µL/min and then remains constant with increasing pump rate. K_d also increases as pump rate increases from 5 to 400 µL/min for calcite, whereas it remains constant after 150µL/min for aragonite (Figure 6b).

3.2 XANES analysis

XANES analysis was used to confirm the oxidation state of Cr incorporated into calcite, aragonite, and ACC. Spectra for Cr(VI)-containing phases show a dominant pre-edge peak at ~5989 eV due to the 1s to 3d electronic transition. In contrast, as Cr(III) occurs

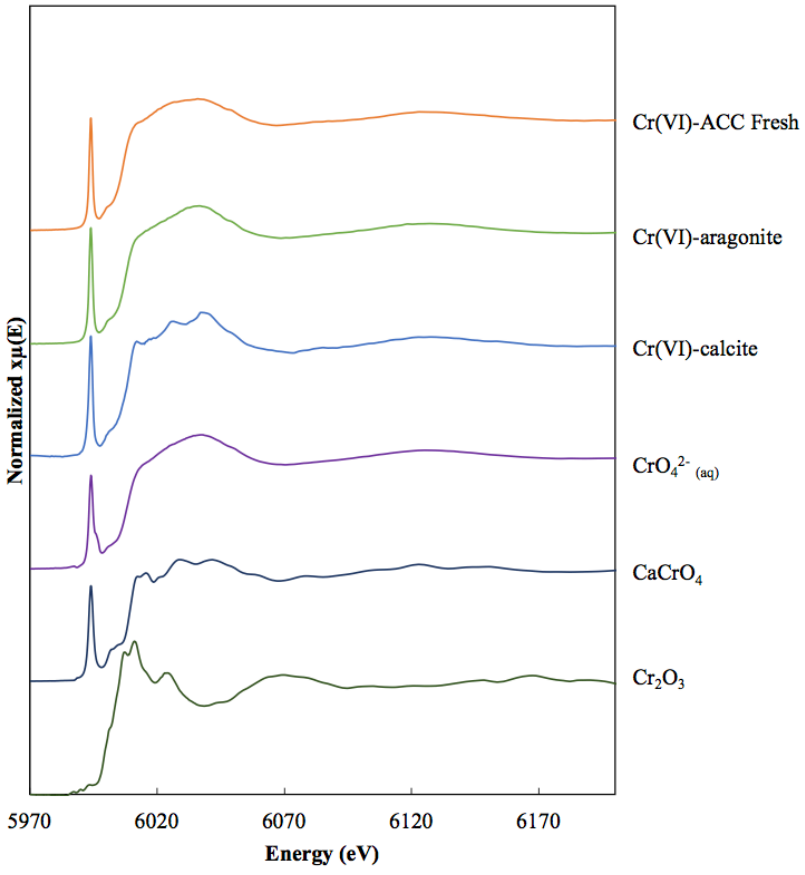

Figure 7: XANES spectra of Cr(VI)-doped aragonite, calcite, and ACC, as well as reference compounds Cr_2O_3, $CaCrO_4$, and CrO_4^{2-} (aq).

almost entirely as octahedral coordination, this transition is less likely thus the absence of this pre-edge peak (Burns, 1993). If Cr(III) is present in the structure, the height of the pre-edge peak would decrease and the edge position would shift to lower energy (Patterson et al., 1997; Peterson et al., 1997; Zachara et al., 2004). The ratio between the pre-edge peak height and normalized edge step can be used to determine the relative abundance of Cr(VI) and Cr(III) in samples (Patterson et al., 1997; Peterson et al., 1997; Zachara et al., 2004). Figure 7 shows the XANES spectra of Cr-doped calcite, aragonite, ACC, and Cr(III) and Cr(VI) reference compounds (Cr_2O_3, $CaCrO_4$, and CrO_4^{2-}). Cr-doped calcite, aragonite, and ACC samples all show a significant pre-edge peak at the same position and similar height as that of $CaCrO_4$ and CrO_4^{2-}, suggesting no redox reactions occurred during the coprecipitation process, consistent with previous study on chromate incorporation into calcite (Tang et al., 2007).

3.3 Cr isotopic fractionation

Isotopic fractionation measurements of incorporated Cr were performed on the three different mineral phases. For calcite, the fractionation measurements were between +0.14 and +0.28‰, for aragonite, were found to be -0.33 and -0.18‰, and for ACC, were -0.14 and +0.07‰ (Figures 8 and 9). Overall, mineral phase, pump rate, and Cr(VI) concentration all affect the direction and amplitude of Cr(VI) isotope fractionation.

Calcite had fractionation values all greater than 0, whereas aragonite had fractionation values close to or less than 0 (Figures 8 and 9). ACC had fractionation measurements that averaged around 0‰ (-0.15 to +0.08‰) compared to aragonite (-0.35 to -0.18‰) or calcite (+0.14 to +0.30‰).

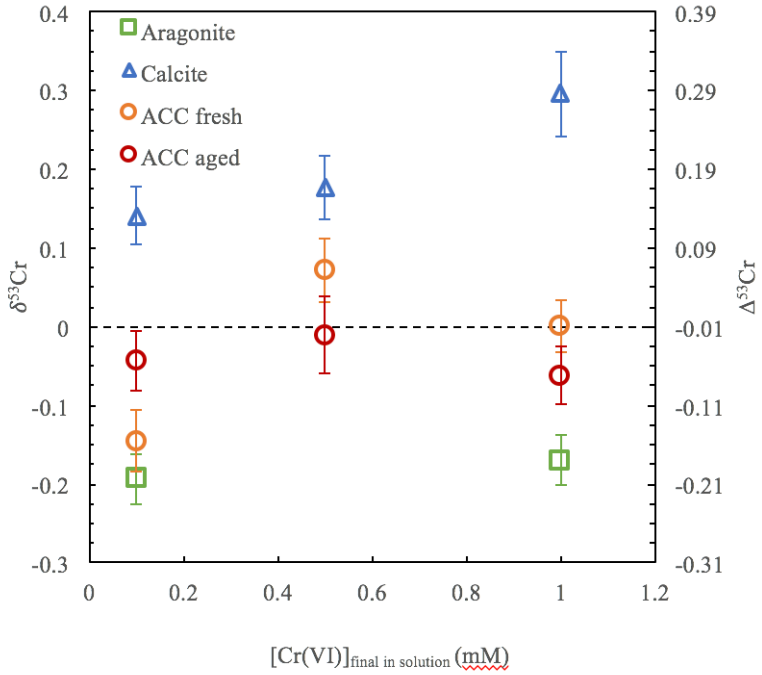

Figure 8: $\delta^{53}Cr$ and $\Delta^{53}Cr$ of Cr(VI)-doped aragonite, calcite, and ACC samples synthesized at varied Cr(VI) initial concentrations. Error bars represent 2σ.

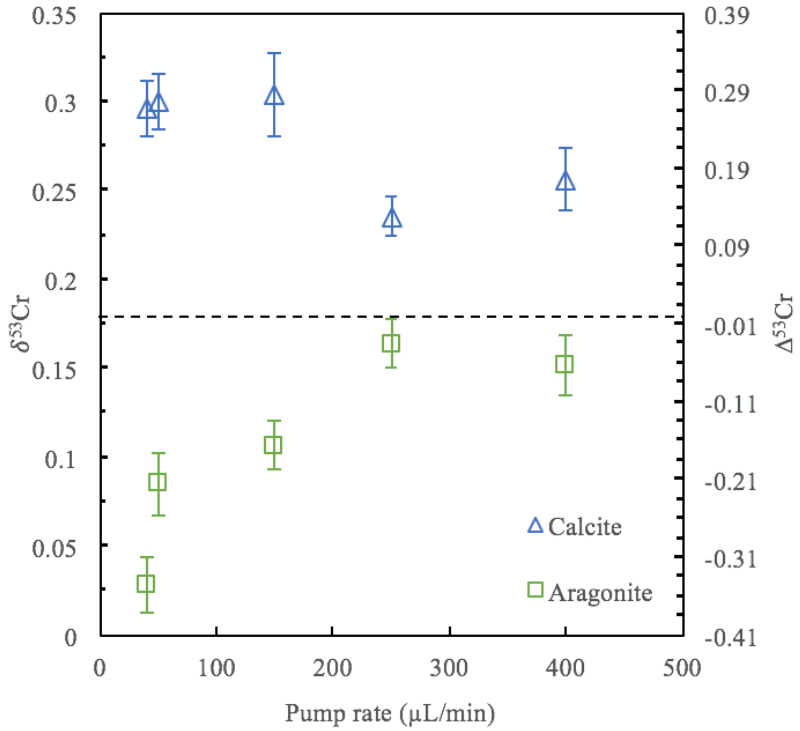

Figure 9: $\delta^{53}Cr$ and $\Delta^{53}Cr$ of Cr(VI)-doped aragonite and calcite samples synthesized at varied pump rate. Error bars represent 2σ.

A change in initial Cr(VI) addition to the bulk solution also varied the fractionation signature in aragonite, calcite, and ACC. In general, fractionation signals became more positive with increasing Cr(VI) initial concentration for calcite and aragonite. ACC does not have a change in fractionation signal with change in Cr(VI) initial concentration. For calcite, the lowest Cr(VI) concentration, 0.1mM, was associated with the most negative calcite fractionation signature (+0.14‰) and increased with increasing Cr(VI) concentration (+0.28‰ at 1mM Cr(VI); Figure 8). For aragonite, the lowest Cr(VI) concentration, 0.1mM, was associated with the most negative aragonite fractionation signal (-0.21‰) and increased with increasing Cr(VI) concentration (-0.18‰ at 1mM Cr(VI); Figure 8). For ACC there was not a clear trend with increasing concentration and associated isotopic fractionation signal. At low Cr(VI) concentration (0.1mM), the fractionation signal was -0.14‰ while an increased Cr(VI) concentration (1mM) the fractionation signal was 0.00‰ (Figure 8).

Pump rate varied the fractionation signal in aragonite and calcite. ACC experiments were conducted at a consistent rate, so pump rate in ACC Cr fractionation signal could not be investigated. At low pump rates, aragonite had a fractionation signal of -0.35‰ at 40µL/min and increased to -0.05‰ at 400 µL/min (Figure 9). A similar trend, fractionation magnitude decreases approaching zero, was seen for calcite, at low pump rates the fractionation signature was +0.28‰ at 50µL/min and decreased to +0.19‰ at 400µL/min (Figure 9).

CHAPTER 4

DISCUSSION

4.1 Incorporation of chromate into calcium carbonate mineral phases

The speciation of Cr(VI) at pH 8.2 is CrO_4^{2-} as confirmed by PHREEQC calculations. SEM and XRD confirmed aragonite, calcite, and ACC were formed during experimentation. The production of aragonite spiked morphology on the high precipitation rate 400µL/min calcite experiment can be observed in both the XRD (Figures 2 and 3) and SEM (Figure 4) results. Although there was no Mg^{2+} present in the calcite experiments, aragonite may have produced due to the rapid nucleation and formation of the calcite (Given and Wilkinson, 1985).

Calcite, aragonite, and ACC were all studied to determine the change in chromate incorporation into the carbonate position as evident in the XANES results. From the results, calcite has the least incorporation whereas aragonite and ACC have more CrO_4^{2-} incorporation into their structures. This is likely due to the structural flexibility differences between calcite, aragonite, and ACC. The porous non-continuous structure of ACC allows for more incorporation of the larger chromate anion as opposed to the carbonate anion. The CaO_9 for aragonite allows for more space within the crystalline structure to accommodate the larger chromate anion relative to the carbonate ion. The incorporation process of chromate into calcite is most likely similar to one of the two methods proposed by Reeder et al. (1994) for SeO_4^{2-} incorporation into calcite. The first is the axial position where the base of the tetrahedral takes the place of the carbonate molecule, and the second is rotated 35 degrees around one O-O bond which was proposed to have less strain on calcite crystal

lattice. Both mechanisms are possible for the incorporation of chromate, and the strain induced from the tetrahedral incorporation into a trigonal planar site is the main difference for incorporation into aragonite, calcite, and ACC. The structure of calcite is more rigid whereas the structure of aragonite and ACC are less rigid.

Calcite, aragonite, and ACC were also studied at various chromate concentrations from 0.005mM to 5mM. In general, as the chromate concentration is increased in the final solution, the concentration of chromate within the solid increases (Figure 5a). Although general trends were observed for aragonite, calcite, and ACC incorporation due to mineral structure, there were some discrepancies in the general trend at varying concentrations as described above. Previous studies have observed that an increase in incompatible ion concentration, such as chromate and sulfate, increases the amount of incompatible ion incorporated into calcite structure (Staudt et al., 1994; Tang et al., 2007). It has been found that cations and anions incorporation into calcite is similar except cations incorporate at the Ca^{2+} site and anions incorporate at the carbonate site. Both cations and anions that are incompatible increase in concentration when the surrounding concentration is increased whereas compatible ions decrease in concentration when the surrounding concentration is increased (Alexandratos et al., 2007; Kitano et al., 1978; Staudt et al., 1994; Tang et al., 2007).

Pump rate of aragonite and calcite were varied from 5 to 400μL/min during the constant addition method described previously. In general, as the pump rate increased, the concentration of chromate within calcite structure increased as well. For aragonite, it appears that the concentration of chromate is consistent with pump rates higher than 150μL/min. The increase in pump rate may reflect an increase in kink sites and therefore

allow for more incorporation (Busenberg and Plummer, 1985). It is believed that precipitation rate is positively correlated to pump rate, but further experimentation and measurements would be needed to quantitatively define this relationship. Other studies have found no correlation between growth rate and incorporation of anions such as sulfate (Staudt et al., 1994).

4.2 Partition coefficient

The partition coefficient results can be found in Figure 5b and Figure 6b. It can be noted that the partition coefficient for calcite is lower than the partition coefficient for aragonite and ACC. This is similar to the results observed for the chromate concentration within the solid and reflects the differences in the crystalline structure between calcite, rigid, and aragonite and ACC, more flexible.

Calcite precipitation at various pump rates was also examined and found that as the pump rate increased the partition coefficient also increased. Aragonite precipitation at various pump rates was examined and found as pump rate increased, up to 150μL/min, the partition coefficient also increased; pump rates greater than 150μL/min resulted in similar Cr(VI) concentrations within the solid. This trend has been observed in other cation (Lorens, 1981; Mavromatis et al., 2013; Pingitore Jr. and Eastman, 1986; Pingitore and Eastman, 1984) and anion (Busenberg and Plummer, 1985) metal incorporation studies. It is likely that the same mechanism that increases incorporation of chromate into calcite and aragonite is responsible for increasing the partition coefficient of chromate in aragonite and calcite at higher precipitation rates.

Although we did not see an apparent trend for chromate concentration and partition coefficient, it has been observed in previous studies that increased chromate concentration in the bulk solution has corresponded with decreased partition coefficient (Tang et al., 2007). Other previous studies have shown decreased partition coefficient with increasing metal concentration including magnesium (Mucci and Morse, 1983) and boron oxyanion (Hemming et al., 1998) in calcite coprecipitation experiments. We may not have seen the same results as our concentrations used were smaller than previous studies have investigated.

4.3 Cr isotope fractionation

Isotope fractionation was found in this study to vary by factors including mineral phase, pump rate, and $Cr(VI)_{final\ in\ solution}$ concentration. Below each factor will be discussed independently and expanded upon for differences in the fractionation observed from these factors.

Few studies have investigated incorporation and associated fractionation of chromium in synthetic calcite at rapid and slow precipitation rates (Rodler et al., 2015). Carbonate samples have shown enrichment in ^{53}Cr as observed in this study (Dixon et al., 2013). However, carbon and oxygen isotopic fractionation in calcite and aragonite have been previously studied. It has been noted that ^{13}C and ^{18}O are preferentially incorporated due to mineralogical effects (Jimenez-Lopez et al., 2001), and it has been observed that precipitation rate did not influence isotopic partitioning for C (Jimenez-Lopez et al., 2001; Romanek et al., 1992). In general, aragonite was enriched in ^{13}C by 1.7 ‰, and ^{18}O by 1.0‰ as compared to calcite which is opposite of what we observed in this study (Bohm

et al., 2000; Romanek et al., 1992). Cations, such as Mg, have also been investigated for incorporation and associated fractionation into calcite (Mavromatis et al., 2013). Mavromatis et al. (2013) observed enrichment of ^{26}Mg with decreasing precipitation rate and increasing partition coefficient.

The change in directionality and magnitude for Cr isotopic fractionation is most likely caused by the differences in crystalline structure of the various carbonate mineral phases. Positive fractionation corresponds to heavier chromate anions indicating enrichment of ^{53}Cr chromate anions with regards to the reference material whereas negative fractionation corresponds to enrichment of ^{52}Cr anion (Equation 3). The distance between the ^{53}Cr-O and ^{52}Cr-O is shorter because ^{53}Cr atom has a larger mass, therefore positive fractionation (Equation 3) and enrichment of ^{53}Cr is associated with a smaller tetrahedral as opposed to $^{52}CrO_4^{2-}$ tetrahedral (Schauble, 2004). Calcite and aragonite have repeatable continuous crystalline structures where aragonite has larger capacity for larger ions due to CaO_9 organization. ACC has medium range order with many Ca-poor channels amongst a Ca-rich framework, and in these channels water and carbonate molecules exist; the Ca found within the framework has a coordination number between 3 and 9 (Goodwin et al., 2010). The larger coordination numbers allow for more incorporation of larger anions due to increased space between carbonate groups, and this allows easier tetrahedral incorporation at a trigonal planar site as observed in borate coprecipitation into calcite and aragonite (Kitano et al., 1978). Iron incorporation and associated isotopic fractionation has also been studied and observed to increase in fractionation in more rigid structures (Balci et al., 2006). The smaller magnitude in fractionation observed in ACC (-0.14 to +0.09‰) as compared to aragonite (-0.33 and +0.02‰) and calcite (+0.14 and +0.28‰) is due to the

large poor space within ACC structure and the various coordination numbers of calcium. The flexibility allows for chromate anions to incorporate both as $^{52}CrO_4^{2-}$ and $^{53}CrO_4^{2-}$ as size is not as important of a factor for incorporation into ACC. The positive fractionation signatures observed with calcite incorporation (Figures 8 and 9) is likely representative of the smaller space allowed for substitution in calcite when compared to aragonite and ACC (Equation 3).

Changes in pump rate also influence the amount of fractionation of incorporated Cr into calcium carbonate mineral phases. As pump rate was increased, the fractionation signal decreased, less fractionation from original source, for aragonite (-0.2 to -0.05‰) and calcite (+0.28 to +0.19‰). This is similar to findings in Mavromatis et al. (2013) that found decreased enrichment of ^{26}Mg with increasing precipitation rate. Most of the isotopic fractionation measured in their study was assumed to be from kinetic isotopic fractionation, not equilibrium isotopic fractionation, due to the rates of precipitation and previous calculations done by Young and Galy (2004). Kinetic isotopic fractionation results in isotopic fractionation signals from processes such as rate of crystal growth or rate of reaction process. As precipitation rate is increased, the faster growth kinetics result in faster kink site attachment as modeled by DePaolo (2011) for cation incorporation into calcite. These results predict that lighter isotopes will preferentially incorporate at higher precipitation rates due to their faster transport and attachment to the surface (DePaolo, 2011). Although this trend follows that of chromate incorporation into calcite, enriching the solid in lighter ^{52}Cr at higher precipitation rates, this trend does not follow for aragonite. Instead, we propose that at precipitation rates experienced in this study exceed transport

kinetics and are dependent upon growth kinetics therefore incorporation is not isotopically selective at high precipitation rates.

Change in Cr(VI) initial concentration also influenced the amount of Cr fractionation of in calcium carbonate mineral phases. The concentrations in natural systems range from 2-10 nM, but concentrations this low would not be accurately measured and we aim to show that Cr isotopic fractionation changes when the surrounding Cr(VI) concentration changes. In general, increasing Cr(VI) concentration shows fractionation more positive in aragonite (-0.49‰ to +0.05‰) and calcite (+0.15‰ to +0.29‰) at 0.1mM and 5mM, respectively. In previous discussion, incorporation of Cr(VI) has been shown to increase when the surrounding Cr(VI) concentration is increased (Tang et al., 2007). SeO_4^{2-} and SO_4^{2-} incorporation into calcite have been previously studied and found that SO_4^{2-}, the smaller tetrahedral, was incorporated more easily than SeO_4^{2-} (Staudt et al., 1994). This concept can be applied to the chromium isotope fractionation measured in this study. Smaller tetrahedrals, such as SO_4^{2-} and $^{53}CrO_4^{2-}$, will be more easily incorporated into calcite and aragonite as opposed to SeO_4^{2-} or $^{52}CrO_4^{2-}$. At higher Cr(VI) concentrations, incorporation of the easier $^{53}CrO_4^{2-}$ will be preferential. This can be noted in the data as increase in Cr isotope fractionation for aragonite, calcite, and ACC (Figure 8). Another possible explanation for the increased positive fractionation with increased Cr concentration is a kinetic effect of transport limited or growth limited processes described above (DePaolo, 2011). This would allow the greater availability of Cr to incorporate and the incorporation of Cr is then limited by the rate of crystallization and precipitation. From the data, it is suggested that there was no correlation with Cr(VI) concentration and Cr isotopic fractionation during ACC incorporation.

CHAPTER 5

CONCLUSIONS AND IMPLICATIONS

This study examined the incorporation of chromate into calcite, aragonite, and ACC during crystal growth and the associated Cr isotope fractionation. Batch experiments showed that $[Cr]_{solid}$ increased with increasing $[Cr]_{solution}$. Partition coefficient values, K_d, overall did not have a clear trend with $[Cr]_{solution}$ changes which may have been due to the lower concentrations of Cr(VI) used in this study compared to previous studies. XANES confirmed that Cr(VI) did not undergo reduction during the incorporation process.

This work is an important consideration in applications of Cr incorporation and Cr isotope fractionation. This provides evidence that incorporation of chromate is different in aragonite, calcite, and amorphous calcium carbonate which may provide insight into other anion incorporation into other carbonate mineral phases. As found in previous studies, our results indicate that incorporation of chromate occurs at the carbonate site in calcite and aragonite and remains Cr(VI) during incorporation (Tang et al., 2007). These results agree with previous anion incorporation work that increased anion solution concentration does increase incorporation (Alexandratos et al., 2007; Kitano et al., 1978; Staudt et al., 1994; Tang et al., 2007). The pump rate increase and associated increase in incorporated anions in this study have been seen in previous studies (Busenberg and Plummer, 1985), but others have found no correlation between pump rate and incorporation of trace elements (Staudt et al., 1994). We cannot determine from this study the mode of incorporation of chromate tetrahedron into calcite or aragonite structure as proposed by Reeder et al. (1994) for SeO_4^{2-} incorporation into calcite. However, we have offered new insight to confirm that the

incorporation of CrO_4^{2-} into calcite and aragonite occurs at the carbonate site and maintains the Cr(VI) oxidation state.

This study also demonstrates the importance of redox-independent processes (e.g. mineral incorporation) in controlling Cr isotope fractionation, and such processes should be considered when using the Cr isotope system as a paleoproxy for reconstructing atmospheric oxygen levels.

Carbonate sediments could serve as a possible sink for global Cr cycle as shown with our results and previous results (Rodler et al., 2015; Tang et al., 2007). Natural Cr abundance in carbonate sediments is 0.2 μmol/g (Forstner and Wittman, 1979), which is much lower than its natural abundance in reducing sediments, such as shales, 1.7 μmol/g (Forstner and Wittman, 1979; Matzat and Shiraki, 1978) and deep sea clays 1.8 μmol/g (Forstner and Wittman, 1979; Matzat and Shiraki, 1978). For lab synthesized carbonates, concentrations of Cr are much higher; for example, this study presents calcite with 1900 to 3000 μmol/g Cr and aragonite 1900 to 7000 μmol/g. Rodler et al. (2015) synthesized calcite samples with Cr incorporation between 1000 and 10,000 μmol/g. The concentrations for synthesized calcite and aragonite are also exposed to higher Cr concentrations, 0.005 to 5 mM this study, than observed in natural environments, 2-10 nM in marine environments. Although these differences exist, there is possibility that carbonate sediments could serve as a potential sink for Cr and that the trends observed in incorporation and fractionation with pump rate and surrounding Cr(VI) concentration could hold true at environmental concentrations.

The amplitude of fractionation is similar to that found in the previous Cr coprecipitation with calcite from Rodler et al. (2015) ranging from 0.24 to 0.35‰. The

fractionation range for calcite (0.12 to 0.28‰), aragonite (-0.34 to +0.01‰), and ACC (-0.17 to +0.03‰) fall within the range of observed Cr isotope fractionation from previous carbonate studies (Wang et al., 2016). Although the amplitude of Cr isotope fractionation is small within all calcium carbonate phases in this study, this is significant in regards to the paleoproxy as small amounts of fractionation are associated with lower atmospheric oxygen concentrations (Frei et al., 2009; Planavsky et al., 2014a; Reinhard et al., 2014).

The direction of Cr isotope fractionation in previous studies has been found to be both positive (Frei et al., 2009; Planavsky et al., 2014b; Reinhard et al., 2014) and negative (Crowe et al., 2013). This study found that aragonite preferentially incorporated lighter chromate anions as indicated by the negative isotopic signature and calcite preferentially incorporated heavier chromate anions as indicated by the positive isotope signature. The direction of Rodler et al. (2015) Cr isotope fractionation in calcite was also positive, indicative of $^{53}CrO_4^{2-}$ incorporation. The directionality differences in aragonite and calcite are believed to be caused by differences in the crystalline structure. This should be further investigated as different mineral phases may influence isotopic fractionation within trace metals incorporated into their structures. The negative fractionation measured in aragonite samples is also interesting as it provides an additional sink for ^{52}Cr in marine environments. This thesis has given evidence to indicate that Cr fractionation can occur independently of redox reactions, and Cr fractionation and incorporation depend on mineral phase, pump rate, and bulk solution chemistry.

REFERENCES

Adriano, D.C. (1986) Trace Elements in the Environment, Chapter 5: Chromium. Springer - Verlag.

Alexandratos, V.G., Elzinga, E.J. and Reeder, R.J. (2007) Arsenate uptake by calcite: macroscopic and spectroscopic characterization of adsorption and incorporation mechanisms. Geochimica et Cosmochimica Acta, pp. 4172-4187.

Anbar, A.D., Duan, Y., Lyons, T.W., Arnold, G.L., Kendall, B., Creaser, R.A., Kaufman, A.J., Gordon, G.W., Scott, C., Garvin, J. and Buick, R. (2007) A whiff of oxygen before the great oxidation event? Science, pp. 1903-1906.

Apte, A., Tare, V. and Bose, P. (2006) Extent of oxidation of Cr(III) to Cr(VI) under various conditions pertaining to natural environment. Elsevier, Journal of Hazardous Materials, pp. 164-174.

Arnold, G.L., Anbar, A.D., Barling, J. and Lyons, T.W. (2004) Molybdenum isotope evidence for widespread anoxia in mid-proterozic oceans. Science, pp. 87-90.

Bagchi, D., Stohs, S., Downs, B., Bagchi, M. and Preuss, H. (2002) Cytotoxicity and oxidative mechanisms of different forms of chromium. Elsevier, Toxicology, pp. 5-22.

Bain, D.J. and Bullen, T.D. (2005) Chromium isotope fractionation during oxidation of Cr (III) by manganese oxides. Geochimica et Cosmochimica Acta Supplement, p. A212.

Balci, N., Bullen, T.D., Witte-Lien, K., Shanks, W.C., Motelica, M. and Mandernack, K.W. (2006) Iron isotope fractionation during microbially stimulated Fe(II) oxidation and Fe(III) precipitation. Geochimica et Cosmochimica Acta, pp. 622-639.

Baloga, M. and Earley, J. (1961) The Kinetics of the Oxidation of Cr(III) to Cr(VI) by Hydrogen Peroxide, pp. 4906-4909.

Banner, J.L. and Hanson, G.N. (1990) Calculation of simultaneous isotopic and trace element variations during water-rock interaction with applications to carbonate diagenesis. Geochimica et Cosmochimica Acta, pp. 3123-3137.

Bardelli, F., Benvenuti, M., Costagliola, P., De Benedetto, F., Lattanzi, P., Meneghini, C., Romanelli, M. and Valenzano, L. (2011) Arsenic uptake by natural calcite: An XAS study. Geochimica et Cosmochimica Acta, pp. 3011-3023.

Barling, J. and Anbar, A.D. (2004) Molybdenum isotope fractionation during adsorption by manganese oxides. Earth and Planetary Science Letters, pp. 315-329.

Barnhart, J. (1997) Occurrences, Uses, and Properties of Chromium. Regulatory Toxicology and Pharmacology, pp. S3-S7.

Bartlett, R. (1991) Chromium Cycling in Soils and Water: Links, Gaps, and Methods. Environmental Health Perspectives, pp. 17-24.

Bartlett, R. and James, B. (1979) Behavior of chromium in soils: III. Oxidation. Journal of Environmental Quality, pp. 31-35.

Bekker, A. and Holland, H.D. (2012) Oxygen overshoot and recovery during the early Paleoproterozoic. Earth and Planetary Science Letters, pp. 295-304.

Bekker, A., Holland, H.D., L., W.P., Rumbe III, D., Stein, H.J., L., H.J., Coetzee, L.L. and Beukes, N.J. (2004) Dating the rise of atmospheric oxygen. Nature, pp. 117-120.

Bekker, A., Holmden, C., Beukes, N.J., Kenig, F., Eglinton, B. and Patterson, W.P. (2008) Fractionation between inorganic and organic carbon during the Lomagundi (2.22-2.1 Ga) carbon isotope excursion. Earth and Planetary Science Letters, pp. 278-291.

Beniash, E., Aizenberg, J., Added, L. and Weiner, S. (1997) Amorphous calcium carbonate transforms into calcite during sea urchin larval spicule growth. Proceedings of the Royal Society of London B: Biological Sciences, pp. 461-465.

Bohm, F., Joachimski, M.M., Dullo, W.C., Eisenhauer, A., Lehnert, H., Reitner, J. and Worheide, G. (2000) Oxygen isotope fractionation in marine aragonite of coralline sponges. Geochimica et Cosmochimica Acta, pp. 1695-1703.

Bonnand, P., James, R.H., Parkinson, I.J., Connelly, D.P. and Fairchild, I.J. (2013) The chromium isotopic composition of seawater and marine carbonates. Earth and Planetary Science Letters, pp. 10-20.

Buerge, I.J. and Hug, S.J. (1997) Kinetics and pH dependance of Cr(VI) reduction by Iron(II). Environmental Science and Technology, pp. 1426-1432.

Burns, R.G. (1993) Mineralogical applications of crystal field theory, 2nd ed. Cambridge University Press.

Busenberg, E. and Plummer, L.N. (1985) Kinetic and thermodynamic factors controlling the distribution of SO_3^{2-} and Na^+ in calcites and selected aragonites. Geochimica et Cosmochimica Acta, pp. 713-725.

Canfield, D.E. (2005) The early history of atmospheric oxygen: Homage to Robert M. Garrels. Annual Review Earth Planetary Science, pp. 1-36.

Crowe, S., Dossing, L., Beukes, N., Bau, M., Kruger, S., Frei, R. and Canfield, D. (2013) Atmospheric oxygenation three billion years ago. Nature.

DePaolo, D.J. (2011) Surface kinetic model for isotopic and trace element fractionation during precipitation of calcite from aqueous solutions. Geochimica et Cosmochimica Acta, pp. 1039-1056.

Dixon, S.K., Peacock, C.L., Parkinson, I.J., Fehr, M.A. and James, R.H. (2013) A combined isotopic and XAS study of Cr incorporation into marine carbonates: Towards verifying Cr isotopes as a paleoredox proxy. Mineralogical Magazine, p. 1926.

Dossing, L., Dideriksen, K., Stipp, S. and Frei, R. (2001) Reduction of hexavalent chromium by ferrous iron: A process of chromium isotope fractionation and its relevance to natural environments. Chemical Geology, pp. 157-166.

Duan, Y., Anbar, A., Arnold, G., Lyons, T., Gordon, G. and Kendall, B. (2010) Molybdenum isotope evidence for mild environmental oxygenation before the great oxidation event. Geochimica et Cosmochimica Acta, pp. 6655-6668.

Eary, L. and Rai, D. (1987) Kinetics of chromium(III) oxidation to chromium(VI) by reaction with manganese dioxide, Environmental Science and Technology, pp. 1187-1193.

Eaton, A.D., Clesceri, L.S. and Greenberg, A.E. (1995) Standard methods for the examination of water and wastewater, 19th ed. American Public Health Association.

Elderfield, H., Bertram, C.J. and Erez, J. (1996) A biomineralization model for the incorporation of trace elements into foraminiferal calcium carbonate. Earth and Planetary Science Letters, pp. 409-423.

Ellis, A., Johnson, T. and Bullen, T. (2002) Chromium isotopes and the fate of hexavalent chromium in the environment. Science, pp. 2060-2062.

Elzinga, E.J. and Reeder, R.J. (2002) X-ray adsorption spectroscopy study of Cu^2+ and Zn^2+ adsorption complexes at the calcite surface: Implications for site-specific metal incorporation preferences during calcite crystal growth. Geochimica et Cosmochimica Acta, pp. 3943-3954.

Farquhar, J. and Wing, B.A. (2003) Multiple sulfur isotopes and the evolution of the atmosphere. Planetary Science Letters, pp. 1-13.

Fendorf, S.E. (1995) Surface reactions of chromium in soils and water. Geoderma, pp. 55-71.

Forstner, U. and Wittman, G.T. (1979) Metal Pollution in the Aquatic Environment. Springer.

Frei, R., Crowe, S.A., Bau, M., Polat, A., Fowle, D.A. and Dossing, L.N. (2016) Oxidative elemental cycling under the low O_2 Eoarchean atmosphere. Scientific Reports, p. 21058.

Frei, R., Gaucher, C., Poulton, S. and Canfield, D. (2009) Fluctuations in Precambrian atmospheric oxygenation recorded by chromium isotopes, pp. 250-254.

Friedman, G.M. (1964) Early diagenesis and lithification in carbonate sediments. Journal of Sedimentary Research.

Gilleaudeau, G.J., Frei, R., Kaufman, A.J., Kah, L.C., Azmy, K., Bartley, J.K., Chernyavskiy, P. and Knoll, A.H. (2016) Oxygenation of the mid-Proterozoic atmosphere: clues from chromium isotopes in carbonate rocks. Geochemical Perspectives Letters, pp. 178-186.

Given, R.K. and Wilkinson, B.H. (1985) Kinetic control fo morphology, composition, and mineralogy of abiotic sedimentary carbonates. Journal of Sedimentary Research, pp. 109-119.

Goldhaber, M.B. and Kaplan, I.R. (1980) Mechanisms of sulfur incorporation and isotope fractionation during early diagenesis in sediments of the gulf of California. Marine Chemistry, pp. 95-143.

Goodwin, A., Michel, F., Phillips, B., Keen, D., Dove, M. and Reeder, R. (2010) Nanoporous structure and medium-range order in synthetic amorphous calcium carbonate. Chemistry of Materials, pp. 3197-3205.

Hemming, N.G., Reeder, R.J. and Hart, S.R. (1998) Growth-step-selective incorporation of boron on the calcite surface. Geochimica et Cosmochimica Acta, pp. 2915-2922.

Holland, H.D. (2002) Volcanic gases, black smokers, and the Great Oxidation Event. Geochimica et Cosmochimica Acta, pp. 3811-3826.

Holland, H.D. (2006) The oxygenation of the atmosphere and oceans. Philosophical Transactions of the Royal Society, pp. 903-915.

Izbicki, J., Bullen, T., Martin, P. and Schroth, B. (2012) Delta chromium-53/52 isotopic composition of native and contaminated groundwater, Mojave Desert, USA. Applied Geochemistry, pp. 841-853.

Jimenez-Lopez, C., Caballero, E., Huertas, F.J. and Romanek, C.S. (2001) Chemical, mineralogical and isotope behavior, and phase transformation during the precipitation of calcium carbonate minerals from intermediate ionic solution at 25 C. Geochimica et Cosmochimica Acta, pp. 3219-3231.

Johnson, C.M., Beard, B.L. and Roden, E.E. (2008) The iron isotope fingerprints of redox and biogeochemical cycling in modern and ancient Earth. Annual Review of Earth and Planetary Sciences, pp. 457-493.

Karhu, J.A. and Holland, H.D. (1996) Carbon isotopes and the rise of atmospheric oxygen. Geology, pp. 867-870.

Kasting, J.F., Holland, H.D. and Pinto, J.P. (1985) Oxidant Abundances in Rainwater and the Evolution of Atmospheric Oxygen. Journal of Geophysical Research, pp. 10497-10510.

Katz, S.A. and Salem, H. (1994) The Biological and Environmental Chemistry of Chromium. VCH Publishers.

Kitano, Y., Okumura, M. and Idogaki, M. (1978) Coprecipitation of borate-boron with calcium carbonate. Geochemical Journal, pp. 183-189.

Koga, N., Nakagoe, Y. and Tanaka, H. (1998) Crystallization of amorphous calcium carbonate. Thermochimica Acta, pp. 239-244.

Konhauser, K.O., Lalonde, S.F., Planavsky, N.J., Pecoits, E., Lyons, T.W., Mojzsis, S.J., Rouxel, O.J., Barley, M.E., Rosiere, C., Fralick, P.W., Kump, L.R. and Bekker, A. (2011) Aerobic bacterial pyrite oxidation and acid rock drainage during the Great Oxidation Event. Nature, pp. 369-374.

Kontrec, J., Kralj, D., Brecevic, L., Falini, G., Fermani, S., Noethig-Laslo, V. and Mirosavljevic, K. (2004) Incorporation of inorganic anions in calcite. European Journal of Inorganic Chemistry, pp. 4579-4585.

Kotas, J. and Stasicka, Z. (2000) Chromium Occurrence in the Environment and Methods of Its Speciation. Environmental Pollution, pp. 263-283.

Kump, L. (2008) The rise of atmospheric oxygen. Nature, pp. 277-278.

Kump, L.R., Junium, C., Arthur, M.A., Brasier, A., Fallick, A., Melezhik, V., Lepland, A., Crne, A.E. and Luo, G. (2011) Isotopic evidence for massive oxidation of organic matter following the great oxidation event. Science, pp. 1694-1696.

Lamble, G.M., Lee, J.F., Staudt, W.J. and Reeder, R.J. (1995) Structural studies of selenate incorporation into calcite crystals. Physica B: Condensed Matter, pp. 589-590.

Lee, A. and Buller, A.T. (1972) Modern temperate-water and warm-water shelf carbonate sediments contrasted. Marine Geology, pp. M67-M73.

Lindsay, D., Farley, K. and Carbonaro, R. (2012) Oxidation of Cr^{III} to Cr^{VI} during chlorination of drinking water. RSC Publishing, Journal of Environmental Monitoring, pp. 1789-1797.

Lorens, R.B. (1981) Sr, Cd, Mn and Co distribution coefficients in calcite as a function of calcite precipitation rate. Geochimica et Cosmochimica Acta, pp. 553-561.

Lyons, T.W. and Gill, B.C. (2010) Ancient sulfur cycling and oxygenation of the early biosphere. Elements, pp. 93-99.

Lyons, T.W., Reinhard, C.T. and Planavsky, N.J. (2014) The rise of oxygen in Earth's early ocean and atmosphere. Nature, pp. 307-315.

Matzat, E. and Shiraki, K. (1978) Chromium. Springer Verlag, Handbook of geochemistry, elements Cr (24) to Br(35), p. 70.

Mavromatis, V., Gautier, Q., Bosc, O. and Schott, J. (2013) Kinetics of Mg partition and Mg stable isotope fractionation during its incorporation in calcite. Geochimica et Cosmochimica Acta, pp. 188-203.

McKay, J.L. and Pedersen, T.F. (2014) Geochemical response to pulsed sedimentation: Implications for the use of Mo as a paleo-proxy. Chemical Geology, pp. 83-94.

Menadakis, M., Maroulis, G. and Koutsoukos, P.G. (2009) Incorporation of Mg^{2+}, Sr^{2+}, Ba^{2+} and Zn^{2+} into aragonite and comparison with calcite. Journal of Mathematical Chemistry, pp. 484-491.

Milacic, R. and Stupar, J. (2006) Fractionation and oxidation of chromium in tannery waste-and sewage sludge-amended soils. Environmental Science & Technology, pp. 506-514.

Mohanta, J., Holmden, C. and Blanchon, P. (2016) Chromium isotope fractionation between seawater and carbonate sediment in the Caribbean Sea. Goldschmidt Abstracts.

Mucci, A. and Morse, J.W. (1983) The incorporation of Mg^{2+} and Sr^{2+} into calcite overgrowths: influences of growth rate and solution composition. Geochemica et Cosmochimica Acta, pp. 217-233.

Mukhopadhyay, J., Crowley, Q.G., Ghosh, S., Ghosh, G., Chakrabarti, K., Misra, B., Heron, K. and Bose, S. (2014) Oxygenation of the Archean atmosphere: New paleosol constraints from eastern India. Geology, pp. 923-926.

Ohmoto, H. (1996) Evidence in pre-2.2 Ga paleosol for the early evolution of atmospheric oxygen and terrestrial biota. Geology, pp. 1135-1138.

Patterson, R.R., Fendorf, S. and Fendorf, M. (1997) Reduction of hexavalent chromium by amorphous iron sulfide. Environmental Science & Technology, pp. 2039-2044.

Pavlov, A.A. and Kasting, J.F. (2002) Mass-Independent fractionation of sulfur isotopes in Archean sediments: strong evidence for an anoxic Archean atmosphere. Astrobiology, pp. 27-41.

Pereira, N.S., Vogelin, A.R., Paulukat, C., Sial, A.N., Ferreira, V.P. and Frei, R. (2016) Chromium-isotope signatures in scleractinian corals from the Rocas Atoll, Tropical South Atlantic. Geobiology, pp. 54-67.

Peterson, M., Brown, G. and Parks, G. (1997) Oxidation state, local structure, and ab-initio XAFS modeling of chromium in contaminated soils and model compounds. Journal de Physique IV Colloque, pp. C2-781-C782-783.

Pettine, M. and Millero, F. (1990) Chromium speciation in seawater: The probable role of hydrogen peroxide, Limnology and Oceanography, pp. 730-736.

Pingitore Jr., N.E. and Eastman, M.P. (1986) The coprecipitation of Sr^{2+} with calcite at 25˚C and 1 atm. Geochimica et Cosmochimica Acta, pp. 2195-2203.

Pingitore, N.E. and Eastman, M.P. (1984) The experimental partitioning of Ba^{2+} into calcite. Chemical Geology, pp. 113-120.

Planavsky, N., Reinhard, C., Wang, X., Thomson, D., McGoldrick, P., Rainbird, R., Johnson, T., Fischer, W. and Lyons, T. (2014a) Low Mid-Proterozoic atmospheric oxygen levels and the delayed rise of animals, Science, pp. 635-638.

Planavsky, N.J., Asael, D., Hofmann, A., Reinhard, C.T., Lalonde, S.V., Knudsen, A., Wang, X., Ossa, F.O., Pecoits, E., Smith, A.J.B., Beukes, N.J., Bekker, A., Johnson, T.M., Konhauser, K.O., Lyons, T.W. and Rouxel, O.J. (2014b) Evidence for oxygenic photosynthesis half a billion years before the Great Oxidation Event. Nature Geoscience, pp. 283-286.

Politi, Y., Arad, T., Klein, E., Weiner, S. and Addadi, L. (2004) Sea urchin spine calcite forms via a transient amorphous calcium carbonate phase. Science, pp. 1161-1164.

Politi, Y., Metzler, R.A., Abrecht, M., Gilbert, B., Wilt, F.H., Sagi, I., Addadi, L., Weiner, S. and Gilbert, P.U.P.A. (2008) Transformation mechanism of amorphous calcium carbonate into calcite in the sea urchin larval spicule. Proceedings of the National Academy of Sciences, pp. 17362-17366.

Raymond, J. and Segre, D. (2006) The effect of oxygen on biochemical networks and the evolution of complex life. Science, pp. 1764-1767.

Reeder, R. (1983) Crystal chemistry of the rhombohedral carbonates. Reviews in Mineralogy and Geochemistry, pp. 1-47.

Reeder, R.J., Lamble, G.M., Lee, J.F. and Staudt, W.J. (1994) Mechanism of SeO_4^{2-} substitution in calcite: An XAFS study. Geochimica et Cosmochimica Acta, pp. 5639-5646.

Reeder, R.J., Nugent, M., Lamble, G.M., Tait, C.D. and Morris, D.E. (2000) Uranyl incorporation into calcite and aragonite: XAFS and luminescence studies. Environmental Science & Technology, pp. 638-644.

Reinhard, C., Planavsky, N., Robbins, L., Partin, C., Gill, B., Lalonde, S., Bekker, A., Konhauser, K. and Lyons, T. (2013) Proterozoic ocean redox and biogeochemical stasis, PNAS, pp. 5357-5362.

Reinhard, C., Planavsky, N., Wang, Z., Fischer, W., Johnson, T. and Lyons, T. (2014) The isotopic composition of authigenic chromium in anoxic marine sediments: A case study from the Cariaco Basin. Elsevier, Earth and Planetary Science Letters, pp. 9-18.

Renard, F., Montes-Hernandez, G., Ruiz-Agudo, E. and Putnis, C.V. (2013) Selenium incorporation into calcite and its effects on crystal growth: An atomic force microscopy study. Chemical Geology, pp. 151-161.

Rodler, A., Sanchez-Pastor, N., Fernandez-Diaz, L. and Frei, R. (2015) Chromium isotope fractionation during coprecipitation with calcium carbonate. Geochimica Cosmochimica Acta, pp. 221-235.

Rodriguez-Blanco, J.D., Shaw, S. and Benning, L.G. (2011) The kinetics and mechanisms of amorphous calcium carbonate (ACC) crystallization to calcite, *via* vaterite. Nanoscale, pp. 265-271.

Romanek, C.S., Grossman, E.L. and Morse, J.W. (1992) Carbon isotopic fractionation in synthetic aragonite and calcite: effects of temperature and precipitation rate. Geochimica et Cosmochimica Acta, pp. 419-430.

Sass, B.M. and Rai, D. (1987) Solubility of amorphous chromium(III)-iron(III) hydroxide solid solutions. Inorganic Chemistry, pp. 2228-2232.

Schauble, E.A. (2004) Applying stable isotope fractionation theory to new systems. Reviews in Mineralogy and Geochemistry, pp. 65-111.

Scheiderich, K., Amini, M., Holmden, C. and Francois, R. (2015) Global variability of chromium isotopes in seawater demonstrated by Pacific, Atlantic, and Arctic Ocean samples. Earth and Planetary Science Letters, pp. 87-97.

Schidlowski, M., Eichmann, R. and Junge, C.E. (1976) Carbon isotope geochemistry of the Precambrian Lomagundi carbonate province, Rhodesia. Geochimica et Cosmochimica Acta, pp. 449-455.

Scott, C. and Lyons, T. (2012) Contrasting molybdenum cycling and isotopic properties in euxinic versus non-euxinic sediments and sedimentary rocks: Refining the paleoproxies. Chemical Geology, pp. 19-27.

Sheldon, N.D. (2006) Precambrian paleosol and atmospheric CO_2 levels. Precambrian Research, pp. 148-155.

Sikora, E., Johnson, T. and Bullen, T. (2008) Microbial mass-dependent fractionation of chromium isotopes. Geochimica et Cosmochimica Acta, pp. 3631-3641.

Staudt, W.J., Reeder, R.J. and Schoonen, M.A. (1994) Surface structural controls on compositional zoning of SO_4^{2-} and SeO_4^{2-} in synthetic calcite single crystals. Geochimica et Cosmochimica Acta, pp. 2087-2098.

Staudt, W.J. and Schoonen, M.A.A. (1995) Sulfate incorporation into sedimentary carbonates. American Chemical Society.

Tang, Y., Elzinga, E., Lee, Y. and Reeder, R. (2007) Coprecipitation of chromate with calcite: batch experiments and X-ray adsorption spectroscopy. Geochimica et Cosmochimica Acta, pp. 1480-1493.

Tebo, B.M., Bargar, J.R., Clement, B.G., Dick, G.J., Murray, K.J., Parker, D., Verity, R. and Webb, S.M. (2004) Biogenic manganese oxides: Properties and mechanisms of formation. Annual Review of Earth and Planetary Sciences, pp. 287-328.

Tebo, B.M., Johnson, H.A., McCarthy, J.K. and Templeton, A.S. (2005) Geomicrobiology of manganese (II) oxidation. TRENDS in Microbiology, pp. 421-428.

Trail, D., Watson, E.B. and Tailby, N.D. (2011) The oxidation state of Hadean magmas and implications for early Earth's atmosphere. Nature, pp. 79-83.

Wang, X.L., Planavsky, N.J., Hull, P.M., Tripati, A.E., Zou, H.J., Elder, L. and Henehan, M. (2016) Chromium isotopic composition of core-top planktonic foraminifera. Geobiology, pp. 1-14.

Weiss, I.M., Tuross, N., Addadi, L. and Weiner, S. (2002) Mollusc larval shell formation: amorphous calcium carbonate is a precursor phase for aragonite. Journal of Experimental Zoology Part A: Ecological Genetics and Physiology, pp. 478-491.

Wille, M., Kramers, J.D., Nagler, T.F., Beukes, N.J., Schroder, S., Meisel, T., Lacassie, J.P. and Voegelin, A.R. (2007) Evidence for a gradual rise of oxygen between 2.6 and 2.5 Ga from Mo isotopes and Re-PGE signatures in shales. Geochmicia et Cosmochimica Acta, pp. 2417-2435.

Young, E.D. and Galy, A. (2004) The isotope geochemistry and cosmochemistry of magnesium. Reviews in Mineralogy and Geochemistry, pp. 197-230.

Zachara, J.M., Ainsworth, C., Brown Jr., G., Catalano, J. and Mckinley, J. (2004) Chromium speciation and mobility in a high level nuclear waste arose zone plume. Geochimica et Cosmochimica Acta, pp. 13-30.

Zhang, Z., Xie, Y., Xu, X., Pan, H. and Tang, R. (2012) Transformation of amorphous calcium carbonate into aragonite. Journal of Crystal Growth, pp. 62-67.

Zink, S., Schoenberg, R. and Staubwasser, M. (2010) Isotopic fractionation and reaction kinetics between Cr(III) and Cr(VI) in aqueous media. Geochimica et Cosmochimica Acta, pp. 5729-5745.